Applied Radiation and Isotopes 154 (2019) 108878

Contents lists available at ScienceDirect

Applied Radiation and Isotopes

journal homepage: www.elsevier.com/locate/apradiso

Characterization of CsI(Tl) and LYSO(Ce) scintillator detectors by measurements and Monte Carlo simulations

I. Mouhti[a], A. Elanique[a,*], M.Y. Messous[b], A. Benahmed[b], J.E. McFee[c], Y. Elgoub[a], P. Griffith[d]

[a] Laboratory of Condensed Matter and Nanomaterials for Renewable Energy, Faculty of Sciences, University Ibn Zohr Agadir, Morocco
[b] National Center for Energy, Sciences and Nuclear Techniques CNESTEN, Rabat, Morocco
[c] McFysics Consulting, Medicine Hat, Canada
[d] Instituto Nazionale Di Fisica Nucleare Cagliari, Italy

HIGHLIGHTS

- CsI(Tl) and LYSO(Ce) scintillator detectors (10 × 10 × 5 mm) characterized experimentally.
- Energy resolution and detection efficiency measured in photon energy range 60–1332 keV.
- Detector efficiencies computed using Monte Carlo codes MCNPX and Geant4.
- Mathematical models developed for the CsI(Tl) and LYSO(Ce) detectors validated.

ARTICLE INFO

Keywords:
Gamma-ray spectrometry
Inorganic scintillator
CsI(Tl)
LYSO(Ce)
Monte Carlo simulation
Energy resolution
Efficiency
MCNPX
Geant4

ABSTRACT

In this study, we investigated the performance of two cuboid scintillation detectors: thallium-activated cesium iodide [CsI(Tl)] and cerium-doped lutetium yttrium orthosilicate [LYSO(Ce)]. The CsI and LYSO crystals were 5 mm thick with an active area of 10 mm × 10 mm. The LYSO scintillator is characterized by its high stopping power and non-hygroscopicity (neither packaging nor light guide are required). Nevertheless, the main disadvantages of LYSO detectors are a lower light output (32 photons/keV) and an intrinsic radioactivity caused by the β^- decay of ^{176}Lu (half-life 3.78 × 10^{10} years). In contrast, CsI crystals present a relatively high light output (54 photons/keV) allowing better energy resolution; however, the drawback of a CsI detector is low detection efficiency.

First, we measured the photon detection efficiency of each scintillator in the photon energy range of 60–1332 keV using radioactive sources. Second, we computed detector efficiencies using the Monte Carlo codes MCNP and Geant4. A comparison between simulated and measured efficiencies showed a good agreement. This comparison confirmed the validity of the mathematical models developed for the two scintillation detectors CsI (Tl) and LYSO(Ce) under investigation.

1. Introduction

Scintillation detectors constitute a major class of radiation detectors that have been broadly used over many years in gamma-ray spectrometry and nuclear medicine (e.g. PET scanners). The scintillation photons are detected by a photomultiplier tube (PMT) and converted into an electronic signal (Lecoq, 2016). Scintillation detectors generally benefit from high detection efficiency, the ability to measure energy spectra, the possibility to work with very high counting rates (up to 10^7 counts/s) and good time resolution (Moszynski et al., 2016).

Within the inorganic scintillator class, cerium-doped lutetium yttrium orthosilicate LYSO(Ce) crystal is prominent. The LYSO scintillator is characterized by its high stopping power and its non-hygroscopicity (i.e. neither packaging nor light guide are required). It also has advantages of high density (7.1 g/cm^3), quick decay time (45 ns), excellent energy resolution (7.1% at 662 keV) and low cost ($25/cm^3). These properties make LYSO ideal for a range of detection applications in nuclear physics and nuclear medicine (Phunpueok et al., 2012). Nevertheless, the main disadvantages of LYSO detectors are a lower light output (32 photons/keV) and an intrinsic radioactivity caused by the β^- decay of ^{176}Lu radionuclide (natural abundance 2.6%, half-life 3.78 × 10^{10}years) followed by a prompt gamma-ray cascade at energies

* Corresponding author.
E-mail address: a.elanique@uiz.ac.ma (A. Elanique).

https://doi.org/10.1016/j.apradiso.2019.108878
Received 19 February 2019; Received in revised form 20 August 2019; Accepted 23 August 2019
Available online 27 August 2019
0969-8043/

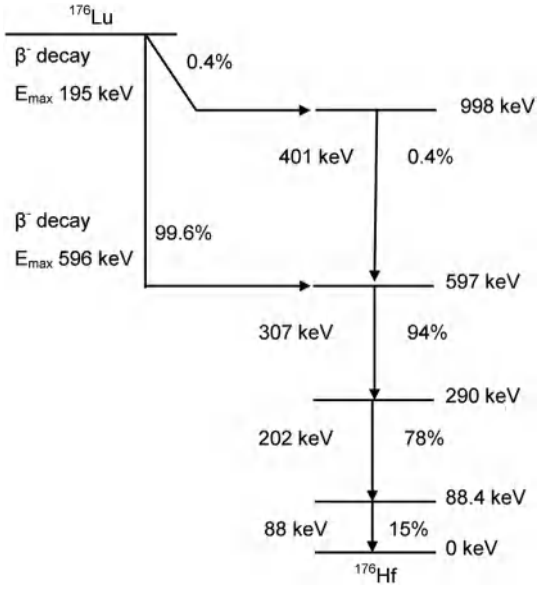

Fig. 1. Simplified decay scheme of ^{176}Lu (natural abundance 2.6%, half-life 3.78×10^{10} years) from Browne and Junde (2002).

of 307 and 202 keV. A simplified decay scheme of ^{176}Lu is shown in Fig. 1 (Browne and Junde, 2002).

In contrast, the thallium-activated cesium iodide CsI(Tl) scintillation detector is among the brightest known inorganic scintillators (54 photon/keV) with the following features: slightly hygroscopic, high density (4.51 g/cm^3), slow decay time (1000 ns), good energy resolution (6% at 662 keV), low cost ($4.5/cm^3) and good mechanical properties.

To date, several Monte Carlo (MC) studies of the response functions of CsI(Tl) and LYSO(Ce) have been performed. Loignon-Houle et al. (2017) calculated the scintillation light output from a single LYSO crystal wrapped in a specular reflector and by simulation through a factorial design evaluated the factors affecting light transport in pixelated PET detectors. Moszynski (2003) studied several crystals, in particular conducting tests of undoped sodium iodide (NaI) and CsI at low temperature. Irfan and Prasad (1973) evaluated the photofractions of a 3″ × 3″ CsI(Tl) crystal from the experimental results of relative photopeak efficiency. Phunpueok et al. (2012) studied the light output and energy resolution of $Lu_{0.7}Y_{0.3}AlO_3$:Ce and $Lu_{1.95}Y_{0.05}SiO_5$:Ce single-crystals with gamma-ray energies in the range of 22.1–1274.5 keV. In addition, Mao et al. (2008) carried out a comparative study of optical and scintillation properties for various inorganic crystal scintillators: pure CsI, sodium-doped CsI, CsI(Tl), Tl-doped NaI, yttrium-doped lead tungstate, Ce-doped lutetium oxyorthosilicate (LSO), LYSO(Ce), bismuth germanate, cerium fluoride and barium fluoride. More specifically, Mao et al. (2008) measured the light output, optical transmittance, UV excitation and photo-luminescence data for samples with dimensions of 1.5 × radiation length. The latter authors also measured the refractive index (for LSO and LYSO samples) and the temperature dependence of the light output.

The Material Sciences unit at CNESTEN laboratory recently acquired CsI(Tl) and LYSO(Ce) scintillation detector samples for which no published data were available. There was therefore a clear need for further investigations concerning these two crystals.

The goal of the present work is to characterize CsI(Tl) and LYSO(Ce) scintillation detectors experimentally and by carrying out MC calculations. We first measured the gamma-ray energy spectra and the photon detection efficiency for CsI(Tl) and LYSO(Ce) scintillators of size 10 mm × 10 mm × 5 mm, with sources ^{22}Na,^{137}Cs, ^{60}Co and ^{241}Am. Secondly, we simulated the efficiency of both detectors with the MC codes MCNP and Geant4 in the photon energy range of 60–1332 keV. The measurements were performed at three distances between the crystal and the source: 0, 2 and 5 cm. Mathematical models for CsI(Tl) and LYSO(Ce) detectors were developed and validated.

2. Materials and methods

2.1. Experimental details

Experimental characterization of the CsI(Tl) and LYSO(Ce) scintillation detectors was performed using standard gamma spectrometry apparatus and experimental setup used is shown in Fig. 2. The CsI and LYSO cuboids crystals (Epic Crystal, China) had a 10 mm × 10 mm surface and were 5 mm thick. The detectors were readout using nuclear instrumentation module electronics. The bottom face of the scintillators was coupled to a photomultiplier (Model B51D01W, Bridgeport Instruments) using optical grease (BC630, Saint-Gobain). The top and lateral surfaces of the scintillators were wrapped in Teflon and aluminum (Al) foil. The PMT bias high-voltage was supplied by a power supply (Model TC 952A, Tennelec). Signals from the PMT were sent to a preamplifier (Model 2M2/2, Bicron) and then to an amplifier (Model TC 241, Tennelec) connected to a multi-channel pulse-height analyzer (Multiport II, Canberra).

Each energy spectrum was recorded for a period of 600 s using the Genie-2K spectrum analysis software (Canberra, 2006). The radioactive sources used in the present work are shown in Table 1. The gamma-ray energy range covered 60–1332 keV.

2.1.1. Energy calibration

The energy calibration consists of establishing a proportionality between the channel number C and a known photon energy E. This relationship is not always rigorously linear (Knoll, 2010); indeed a minor degree of nonlinearity may be observed. In this work, several

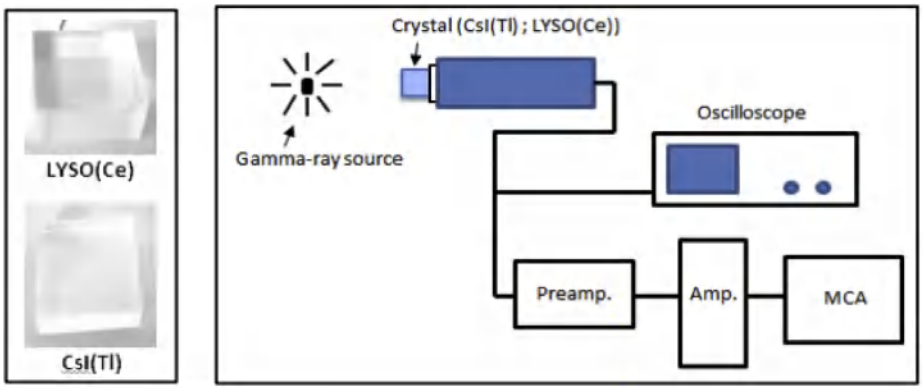

Fig. 2. The experimental set up: left – photographs of the two scintillators investigated; right – block diagram of the electronics readout.

Table 1
Properties of radioactive sources used in the present work.

Radionuclide	Half-life (year)	Energy (keV)	Emission probability (%)	Current activity (kBq)
^{241}Am	432.2	59.54	36.0	2435.71
^{60}Co	5.27	1173.24	99.87	46.9567
		1332.51	99.98	
^{22}Na	2.602	511	100	3.1765
		1274.54	99.94	
^{137}Cs	30.07	661.65	84.6	119.14

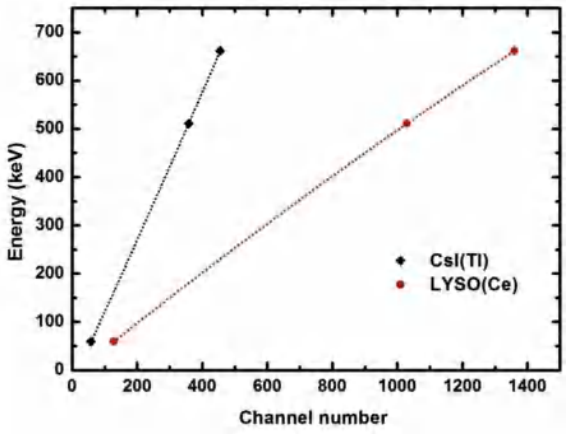

Fig. 3. Energy calibration data and curve fit of the 10 mm × 10 mm × 5 mm CsI and LYSO detectors. The dashed lines correspond to a second-order polynomial fit.

radioactive sources were used for this purpose: ^{241}Am, ^{22}Na and ^{137}Cs sources, as they produce gamma-ray energies of 59.54, 511 and 662 keV, respectively. The energy calibration data and curve fit of the 10 mm × 10 mm × 5 mm CsI and LYSO detectors are shown in Fig. 3.

To express this nonlinearity, a second-order polynomial was used:

$$E = a + b.\,C + d.\,C^2 \quad (1)$$

Values of a, b and d were calculated using a least-square fit of data points and are summarized in Table 2.

2.1.2. Energy resolution

Another important factor that determines the performance of a detector is its energy resolution. It indicates the ability of a detector to discriminate photons with close energies. Defined as the full width at half maximum (FWHM) of the energy peak (E_0), the energy resolution (R) is often expressed as a percentage and evaluated using the following formula:

$$R = \frac{FWHM}{E_0} \times 100\% \quad (2)$$

As previously discussed (Mouhti et al., 2018), the R of the detectors at energy E was fitted by a power law relationship:

$$R = \alpha.\,E^{\beta} \quad (3)$$

where the values of α and β coefficients were obtained by a least-square fit.

Table 2
Values of a, b and d coefficients obtained for the energy calibration – see Eq. (1).

Coefficients	CsI(Tl)	LYSO(Ce)
a	−25.472	−9.601
b	1.454	0.544
d	1.214×10^{-4}	-3.728×10^{-5}

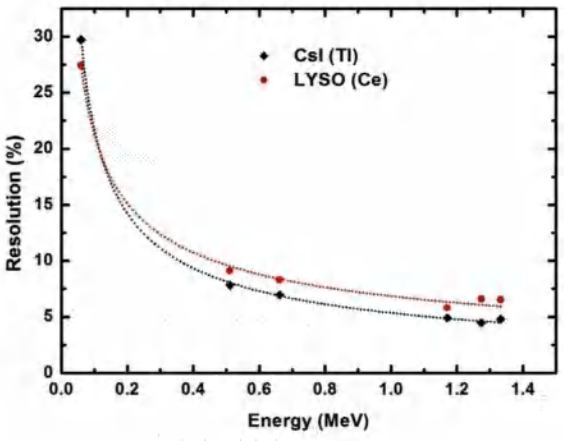

Fig. 4. Experimental data and curve fits for the energy resolution of the CsI(Tl) and the LYSO(Ce) detectors. The dashed lines represent a power law polynomial fit – see Eq. (3).

Fig. 4 shows the experimental data and curves fits for the energy resolution of the CsI and LYSO detector under investigation. The mean energy resolution at 662 keV in the case of the LYSO(Ce) detector is 8.3% while its value is around 7% for the CsI(Tl) crystal. The energy resolution of the CsI detector is roughly 15% higher than that of the LYSO detector in the photon energy range of 150–1400 keV. This is caused mostly by Poisson statistics: the LYSO crystal produces 40% less visible light compared to the CsI crystal (Table 3).

To better illustrate the differences between the CsI(Tl) and LYSO (Ce) crystals, we plotted their mass attenuation coefficient as function of gamma-ray energy (Fig. 5). The plots were obtained with Visual Editor program included in the MCNPX code. Unlike the LYSO(Ce) crystal, the CsI(Tl) combines a high light output (Table 3) with a very high attenuation coefficient (Fig. 5), allowing significant reduction in the thickness of the scintillator required to detect gamma rays and therefore to make smaller detectors.

2.1.3. LYSO background energy spectrum

Of particular interest is the background radiation spectrum of the LYSO scintillator, without external activity, which was recorded for 10 min (Fig. 6). With a low count rate of 140 Bq, the latter is basically related to the intrinsic activity of ^{176}Lu (Fig. 1), which undergoes β-decay to excited states of ^{176}Hf (with maximum β-particle energy of 593 keV). This leads to simultaneous detection of the β-particle plus 88 keV gamma-ray, β-particle plus 202 keV gamma-ray and β-particle plus 307 keV gamma-ray, respectively (Yamamoto et al., 2005). Thus, broad peaks, due to beta continuum, would be expected at 88, 290 (88 + 202), 395 (88 + 307) and 597 keV (88 + 202 + 307). In a recent paper (Alva-Sánchez et al., 2018), MC calculations indicated that all resulting β-particles and internal conversion electrons deposit their whole energy within the crystal – these authors also provide more detailed explanation on the structure of the intrinsic activity of LSO/LYSO detectors.

2.1.4. Experimental efficiency

Photon detection efficiency is a key factor when carrying out

Table 3
Basic properties of the scintillators used in the present work.

Crystal	Density (g/cm^3)	Light yield (photons/keV)	Decay time (ns)	Peak emission wavelength (nm)
CsI(Tl)	4.51	54	1000	550
LYSO(Ce)	7.2	32	40	402

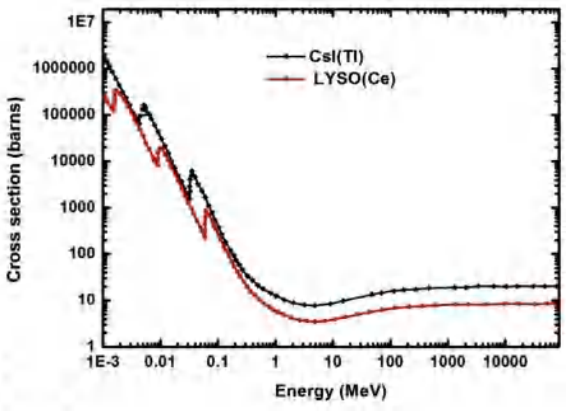

Fig. 5. Mass attenuation coefficients for CsI(Tl) and LYSO(Ce) scintillators. The difference is much more pronounced at energies above 200 keV. The plots were obtained with Visual Editor program included in the MCNPX code.

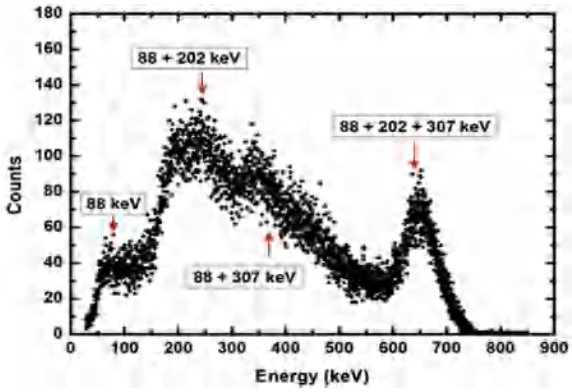

Fig. 6. Measured background radiation spectrum for the LYSO(Ce) scintillator.

accurate quantitative gamma-ray spectrometry. It depends on detector properties and counting geometry (source–detector distance and solid angle subtended by the detector). As reported by Knoll (2010), the absolute photopeak efficiency (ε) of a detector at a certain gamma-ray energy "E" is determined from Eq. (4):

$$\varepsilon = \frac{N}{t.P.A} \tag{4}$$

in which N indicates the measured net photopeak area (counts), t is acquisition time (s), P is photon emission probability and A represents activity of the gamma source at the time of measurement (Bq).

In practice, N is derived by fitting a Gaussian function to the peak of interest, after background subtraction via an advanced algorithm using the Genie-2K software.

2.2. MC simulation

2.2.1. MC codes

The MC calculation has been used for many decades to solve radiation transport problems that may not have analytical solutions. Its use has increased significantly in recent years. Based on random number generation, MC is a statistical method allowing one to virtually carry out a "computer experiment" without handling any radioactive material and to provide reliable computational results (Elanique et al., 2012; Mouhti et al., 2018). Thanks to the powerful advances in computing speed and capabilities, several MC programs have been developed for particle transport, including MCNP (Briesmeister, 2000), Geant4 (Agostinelli et al., 2003), EGSnrc (Kawrakow, 2000) and PENELOPE (Baro et al., 1995). Despite their apparent differences, these MC radiation transport codes rely on simulation of a statistical process, like the interaction of a particle with matter. Each source-particle (e.g. photon or electron) is tracked from creation until death (escape or absorption) with all interactions based on physics models and cross-sections for physics processes (photoelectric absorption, Compton scattering and pair production) and all decisions (interaction point location or scattering angle) are based on pseudo-random numbers (Hendricks et al., 2000).

In the present work, we used MC simulation codes MCNP (version X) and Geant4 (version 10.4 patch1) to study the response function of the CsI and LYSO detectors. Originally developed by the Los Alamos Laboratory (Pelowitz, 2008), MCNP is a general purpose MC N-particle code used for transport simulation of thermal and fast neutrons, photons and electrons in geometries or complex three-dimensional configurations. The MCNP is rather straightforward and has various features including source description, flexible tally (MCNP results) and variance reduction techniques. More specifically, to model the response function of a detector, the user just defines an input ASCII file in which the experimental setup (geometry and materials, physics interaction, number of generated events) is described and specifies the calculated tally (Pelowitz, 2008).

Geant4, however, is an entirely free and open-source simulation toolkit based on object-oriented technology for modeling the interactions of particles with matter. Developed in 1993 by an international collaboration of physicists and software engineers, Geant4 was initially intended for the High Energy Physics community at CERN (Switzerland) and later extended to other physics fields including space science and medical physics. Nowadays, Geant4 is routinely used, inter alia, to design and characterize novel detector systems (Agostinelli et al., 2003). Briefly, the Geant4 code consists of a full set of C++ libraries allowing users to simulate their own experimental setup by developing a Geant4 application. More extensive and updated documentation about the code is provided by the Geant4 web site: http://cern.ch/geant4.

2.2.2. Modeling the detectors

The mathematical model of the CsI and LYSO detectors consisted of a cuboid crystal of 10 mm × 10 mm surface and is 5 mm thick. Its top and lateral surfaces were wrapped in an MgO reflector (0.018 cm thick), Teflon tape (0.013 cm thick) and Al foil (0.002 cm thick) constituting the crystal container (Fig. 7). The point-like sources of mono-energetic photons were positioned, on the detector axis of symmetry, at source–detector distances (d) of 0, 2 and 5 cm, respectively. The basic physical properties of the CsI and LYSO scintillators are summarized in Table 3. The crystals masses, determined by MCNP code, are 2.25 g for the CsI(Tl) detector and 3.6 g for the LYSO(Ce).

The thickness of these three absorbing layers (MgO reflector, Teflon

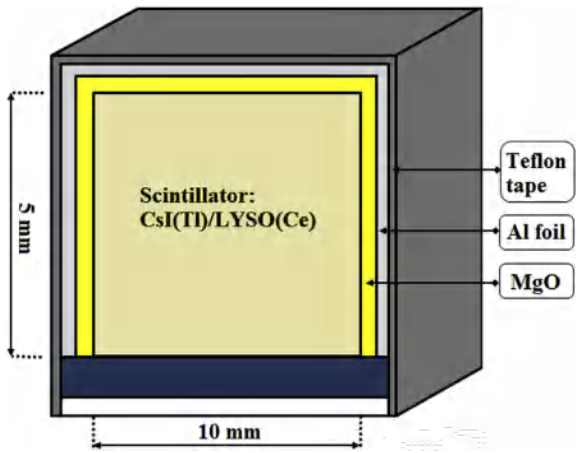

Fig. 7. Schematic diagram of the detector geometry used in the MC simulations. Dimensions are not to scale.

tape and Al foil) is critical for detector efficiency at short source–detector distances (especially at d = 0 cm, which is very sensitive), their composition seems however irrelevant. Thus, at the energies and thicknesses of material of interest, gamma absorption by the container is negligible. For example, transmission through an Al layer of 0.033 cm thickness is 0.976 for 60 keV, 0.994 for 662 keV and 0.995 for 1333 keV.

The distribution of the photon energy deposited in the crystal volume is a pulse-height spectrum (and thus the energy spectrum) which can be computed in MCNP using the "F8" tally (Pelowitz, 2008). Note that MCNP code does not consider optical photons. Instead it just registers the energy released in the crystal, assuming perfect transmission of that energy to the output of the PMT/preamp/amplifier circuit. As a result, in MCNP the pulse-height tally per photon emitted from the source gives the detector efficiency. In Geant4, the efficiency was calculated as the ratio of number of photons contributing to the histogram of a spectral line to the total number of generated events (i.e. histories).

To obtain a reliable statistical error (< 2%), the number of total histories in MCNP simulations was set to 10^7 source particles. Since, the MCNP code does not consider physical effects (optical photon creation) leading to the broadening of the peaks, a Gaussian energy broadening (GEB) option was enabled to mimic experimental spectra (Pelowitz, 2008). The GEB in the energy peak is defined by Eq. (5):

$$\mathrm{FWHM} = \mathrm{f} + \mathrm{g}\sqrt{\mathrm{E} + \mathrm{h}.\ \mathrm{E}^2} \tag{5}$$

where f, g and h are user-provided constants from the fitting function.

The effect of GEB on the pulse-height distribution is clearly observable in Fig. 8, which shows the MCNP calculated energy spectra of a ^{60}Co source (1173.24 and 1332.51 MeV) for CsI(Tl) crystal with and without GEB, respectively. The additional peaks adjacent to the photopeaks for the "perfect" resolution (GEB disabled) in Fig. 8 are due to the escape of the 31 keV Kα1 X-ray of Cs in CsI(Tl) (Knoll, 2010). When a gamma photon undergoes a photoelectric effect close to the edges of the crystal then a characteristic X-ray of energy E_X may escape. Accordingly only a part of the photon energy ($h\nu$) will be deposited inside the scintillator ($E_e = h\nu - E_X$) contributing to a second peak in the energy spectrum.

The Geant4 model employed in this study uses the *G4OpticalPhoton* optical physics list to simulate the generation and transport of scintillation photons. Consequently, unlike the MCNP model, a simulated gamma-ray line has a finite FWHM governed by the number of generated optical photons and transport losses. For 1.173MeV gamma rays, the FWHM is approximately 11 keV in the scintillator and 22 keV at the entrance to the PMT. Given the tiny ratio of the intensity of the escape

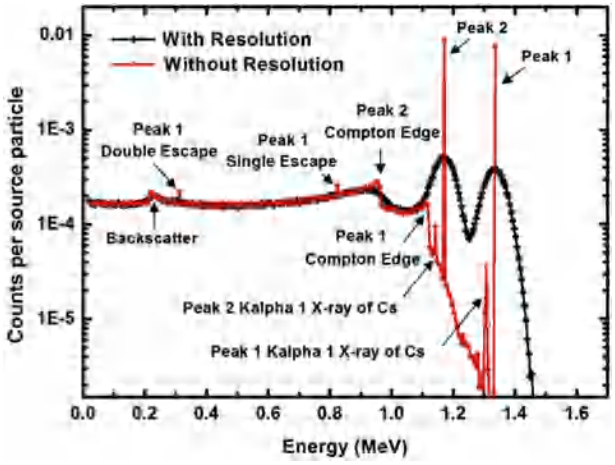

Fig. 8. The pulse-height distribution of a CsI(Tl) scintillator for a ^{60}Co source obtained by the MCNP code considering the effect of Gaussian energy broadening.

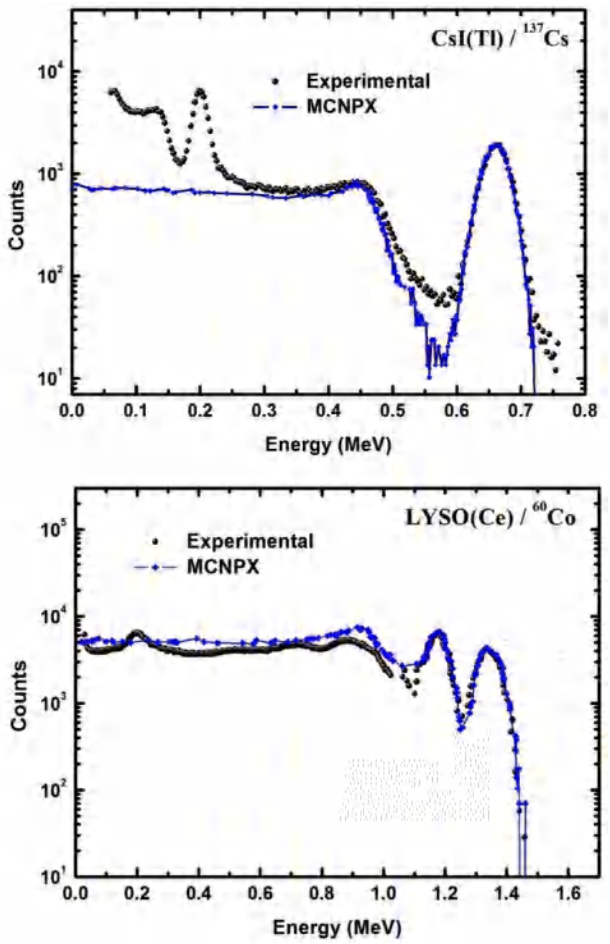

Fig. 9. A comparison of a measured pulse-height spectrum for CsI(Tl) (top) and for LYSO(Ce) scintillators (bottom) with a theoretical spectrum calculated by MCNPX code. The spectra are normalized to the same maximum pulse height.

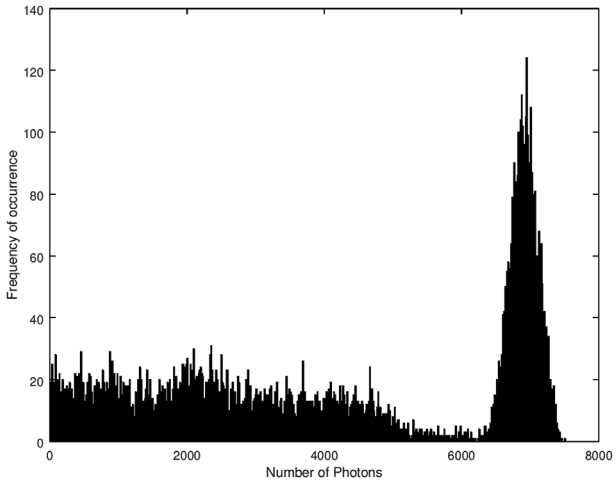

Fig. 10. Histogram of optical photon numbers entering PM front surface resulting from the interaction of a 662-keV gamma-ray within the LYSO scintillator. The spectrum was obtained by Geant4 simulations for 10^5 events. For further details, see text.

Table 4
CsI(Tl) and LYSO(Ce) detector efficiencies obtained both by MC simulation and experiment for various radioactive sources. $RD_M = \frac{\varepsilon_{exp} - \varepsilon_{MCNPX}}{\varepsilon_{exp}}$.$RD_{G4} = \frac{\varepsilon_{exp} - \varepsilon_{Geant4}}{\varepsilon_{exp}}$

Radio nuclide	Source–detector distance (cm)	Energy (keV)	CsI(Tl)				
			ε_{exp}(%)	ε_{Geant4}(%)	RD_{G4}	ε_{MCNPX}(%)	RD_M
^{241}Am	5	60	0.245	0.3042	−0.242	0.265	−0.082
^{22}Na	2	511	0.0865	0.0873	−0.009	0.086	0.002
^{137}Cs	2	662	0.0315	0.0422	−0.339	0.0510	−0.619
	5		0.009	0.0099	−0.100	0.0106	−0.178
^{60}Co	0	1173	0.373	0.3051	0.182	0.305	0.182
		1332	0.343	0.2401	0.300	0.240	0.299
	5	1173	0.0055	0.0032	0.427	0.0036	0.355
		1332	0.0039	0.0024	0.391	0.0028	0.289

Radio nuclide	Source–detector distance (cm)	Energy (keV)	LYSO(Ce)				
			ε_{exp}(%)	ε_{Geant4}(%)	RD_{G4}	ε_{MCNPX}(%)	RD_M
^{241}Am	5	60	0.290	0.275	0.051	0.298	−0.027
^{137}Cs	2	662	0.095	0.181	−0.905	0.150	−0.579

peak to that of the full energy peak and the 31 keV separation, the escape peak is not visible in the Geant4 simulations.

3. Results and discussion

3.1. Gamma-ray energy spectra

An example of our data is presented in Fig. 9 where the experimental and MC simulated (by MCNPX code) gamma-ray energy spectra of ^{137}Cs and ^{60}Co sources for CsI and LYSO detectors are plotted. The pronounced backscatter peaks at 200 keV (Fig. 9) are most likely due to gamma rays from the source that have first undergone Compton scattering in one of the materials surrounding the crystal. This last process was not modeled by our MC calculations. The calculated photon energy spectra reproduce well those measured for photon energies above 250 keV (see CsI spectrum of Fig. 9). For low-energy photons (< 250 keV), the code underestimates the measured spectrum. This is probably because the MC calculation considers neither the Ba X-ray peak at 32 keV nor the backscattering, due to materials surrounding the crystal (Berger and Seltzer, 1972).

The Geant4 application was run to record the distribution of optical photons. An example of the Geant4 result that illustrates a histogram of optical photon numbers reaching the PM surface after the interaction of a 662 keV γ ray within the LYSO scintillator is shown in Fig. 10. The total number of optical photons generated was set to 27.6 ph/keV, while the energy of maximum emission was 2.95 eV (420 nm). The run consists of 10^5 events generating circa 978.2 scintillation counts/event. However, only 371.72 counts/event effectively reached the PM surface (fraction hitting the PM is 38%).

3.2. Detector efficiency determinations

The experimental photon efficiency for the sources listed in Table 2 were compared with the MC simulated results for CsI(Tl) and LYSO(Ce) detectors at source–detector distances of 0, 2 and 5 cm. The experimental ε_{exp} and the MC calculated efficiencies (ε_{Geant4} and ε_{MCNPX}) for both detectors are shown in Table 4. The systematic relative deviation RD between the computed and measured efficiency values was also determined.

Note that the experimental and simulated data indicate good agreement. However, there is a slight discrepancy (especially at 662 keV and close to the detector) caused most likely by various factors including uncertainties on the activities of the reference sources and source positioning.

4. Conclusion

In the present work, the performances of CsI(Tl) and LYSO(Ce) detectors were investigated as a function of gamma-ray energy. The energy resolution and detector efficiency were measured and modeled by Geant4 and MCNPX MC codes for photon energies of 60, 511, 662, 1772 and 1332 keV. Although the two studied scintillators are of identical size, the efficiency of the LYSO(Ce) detector is superior to that of CsI(Tl) detector at higher energy and slightly better at lower energy. Comparison between experimental and MC efficiency values for each detector shows good agreement.

In regard to detection efficiency results of both (CsI and LYSO) crystals, the discrepancies between MCNP and Geant4 calculations do not exceed 15%. Thus, this work may show that, despite its inability to track optical photons within the crystal, MCNP remains a very useful and powerful tool for performing MC simulations of this type of scintillation detector.

Now that we have fully characterized the CsI(Tl) and LYSO(Ce) detectors and improved our knowledge in running MC codes (MCNP and Geant4), the next steps toward setting up a quantitative gamma-spectroscopy system in the laboratory can be undertaken.

Appendix A. Supplementary data

Supplementary data to this article can be found online at https://doi.org/10.1016/j.apradiso.2019.108878.

References

Agostinelli, S., et al., 2003. Geant4: a simulation toolkit. Nucl. Instrum. Methods A 506, 250–303.
Alva-Sánchez, H., Zepeda-Barrios, A., Díaz-Martínez, V.D., Murrieta-Rodríguez, T., Martínez-Dávalos, A., Rodríguez-Villafuerte, M., 2018. Understanding the intrinsic radioactivity energy spectrum from ^{176}Lu in LYSO/LSO scintillation crystals. Sci. Rep. 8 (17310), 1–7.
Baro, J., Sempau, J., Fernandez-Varea, J.M., Salvat, F., 1995. PENELOPE: an algorithm for Monte Carlo simulation of the penetration and energy loss of electrons and positrons in matter. Nucl. Instrum. Methods B 100, 31–46.
Berger, M.J., Seltzer, S.M., 1972. Response functions for sodium iodide scintillation detectors. Nucl. Instrum. Methods 104 (2), 317–332.
Briesmeister, J.F., 2000. MCNP: A General Monte Carlo N-Particle Transport Code, Version 4C, LA-13709-M. Los Alamos National Laboratory.
Browne, E., Junde, H., 2002. Nuclear data sheets for A = 176. Nucl. Data Sheets 84, 337–486.
Elanique, A., Marzocchi, O., Leone, D., Hegenbart, L., Breustedt, B., Oufni, L., 2012. Dead layer thickness characterization of an HPGe detector by measurements and Monte Carlo simulations. Appl. Radiat. Isot. 70, 538–542.
Hendricks, J.S., Adams, K.J., Booth, T.E., Briesmeister, J.F., Carter, L.L., Cox, L.J.,

Favorite, J.A., Forster, R.A., McKinney, G.W., Prael, R.E., 2000. Present and future capabilities of MCNP. Appl. Radiat. Isot. 53, 857–861.
Canberra Industries Inc, 2006. Genie 2k Spectroscopy Software Manual 3.1.
Irfan, M., Prasad, R.D.G., 1973. Photofractions from experimental relative photopeak efficiencies of a 3"x 3" CsI(Tl) crystal. Nucl. Instrum. Methods 107, 583–588.
Kawrakow, I., 2000. Accurate condensed history Monte Carlo simulation of electron transport. I. EGSnrc, the new EGS4 version. Med. Phys. 27, 485–498.
Knoll, G.F., 2010. Radiation Detection and Measurement, fourth ed. John Wiley & Sons, New York.
Lecoq, P., 2016. Development of new scintillators for medical applications. Nucl. Instrum. Methods A 809, 130–139.
Loignon-Houle, F., Bergeron, M., Pepin, C., Charlebois, S., Lecomte, R., 2017. Simulation of scintillation light output in LYSO scintillators through a full factorial design. Phys. Med. Biol. 62 (2), 669–683.
Mao, R., Zhang, L., Zhu, R.Y., 2008. Optical and scintillation properties of inorganic scintillators in high energy physics. IEEE Trans. Nucl. Sci. 55 (4), 2425–2431.
Moszynski, M., 2003. Inorganic scintillation detectors in γ-ray spectrometry. Nucl. Instrum. Methods A 505, 101–110.
Moszynski, M., Syntfeld-Każuch, A., Swiderski, L., Grodzicka, M., Iwanowska, J., Sibczyński, P., 2016. Energy resolution of scintillation detectors. Nucl. Instrum. Methods A 805, 25–35.
Mouhti, I., Elanique, A., Messous, M.Y., Belhorma, B., Benahmed, A., 2018. Validation of a NaI(Tl) and LaBr3(Ce) detector's models via measurements and Monte Carlo simulations. J. Radiat. Res. Appl. Sci. 4 (11), 335–339.
Report LA-CP-07-1473 Pelowitz, D.B. (Ed.), 2008. MCNPX User's Manual Version 2.6.0. Los Alamos National Laboratory.
Phunpueok, A., Chewpraditkul, W., Limsuwan, P., Wanarak, C., 2012. Light output and energy resolution of $Lu_{0.7}Y_{0.3}AlO_3$:Ce and $Lu_{1.95}Y_{0.05}SiO_5$:Ce scintillators. Procedia Eng. 32, 564–570.
Yamamoto, S., Horii, H., Hurutani, M., Matsumoto, K., Senda, M., 2005. Investigation of single, random, and true counts from natural radioactivity in LSO-based clinical PET. Ann. Nucl. Med. 19 (2), 109–114.